Supporting Information

A Modularization Approach for Linear-shaped Functional Supercapacitors

Yang Huang,[a] Minshen Zhu, [a] Yan Huang, [a] Hongfei Li, [a] Zengxia Pei, [a] Qi Xue, [a] Zhen Liao, [a] Zifeng Wang [a] and Chunyi Zhi*[ab]

Calculations of capacitance, energy density and power density. The areal (C_s, F cm^{-2}) and volumetric (C_V, F cm^{-3}) capacitances of C-SMSC and C-SC yarn were calculated from the corresponding GCD curves at different current density according to equation:

$$C = I\Delta t / \Delta V \quad (1)$$

$$C_S = C / A \quad (2)$$

$$C_V = C / V \quad (3)$$

Where C is the capacitance, I is the discharge current, Δt (s) is the discharge time, ΔV (V) is the discharge voltage range (excluding iR drop), A and V are the total area (cm^2) and volume (cm^3) of the device. The A and V are calculated based on following equation: $A = \pi dL$, $V = \pi r^2 L$, where d is the diameter of the whole device (cm), r is the radius of the whole device (cm), and L is the length of the device (cm).

The length capcitance (C_L, F cm^{-1}) of WO_3 electrodeposited yarn and PPy electrodeposited wire, the areal (C_s, F cm^{-2}) and volumetric (C_V, F cm^{-3}) capacitances of asymmetric C-SC were calculated from the corresponding CV curves at different scan rates according to the following equations:

$$C = \frac{1}{\nu(V_f - V_i)} \int_{V_i}^{V_f} I(V)\mathrm{d}V \quad (4)$$

$$C_L = C / L \quad (5)$$

$$C_S = C / A \quad (6)$$

$$C_V = C / V \quad (7)$$

Where C is the capacitance, ν is the scan rate (V s^{-1}), V_f and V_i are the integration potential limits of the voltammetric curve and $I(V)$ is the voltammetric discharge current, L is the length of WO_3 electrodeposited yarn/PPy electrodeposited wire, A and V are the total area (cm^2) and volume (cm^3) of the asymmetric C-SC.

The volumetric energy density was obtained from the following equation:

$$E_V = \frac{1}{2} \times C_V \times \frac{(\Delta V)^2}{3600} \quad (8)$$

Where E_V (Wh cm^{-3}) is the volumetric energy density, C_V is the volumetric capacitance obtained from equation (7). ΔV (V) is the discharge voltage range.

The power density was calculated from the following equation:

$$P_V = \frac{E_V}{\Delta t} \times 3600 \quad (9)$$

Where P_V (W cm^{-3}) is the volumetric power density, E_V is the volumetric energy density obtained from equation (8) and Δt (s) is the discharge time.

Energy storage mechanism. The energy storage mechanism involved during charging and discharging processes could be mainly attributed to the redox reactions of PPy and WO_3, since they are the active materials loaded on our prototypes. The details of the reactions are described as followed:

For PPy, the capacitive performance is highly depended on the reversible doping-dedoping process as shown in scheme S1. The counter ions with opposite charges would be entrapped or released from the PPy during charging and discharging process.

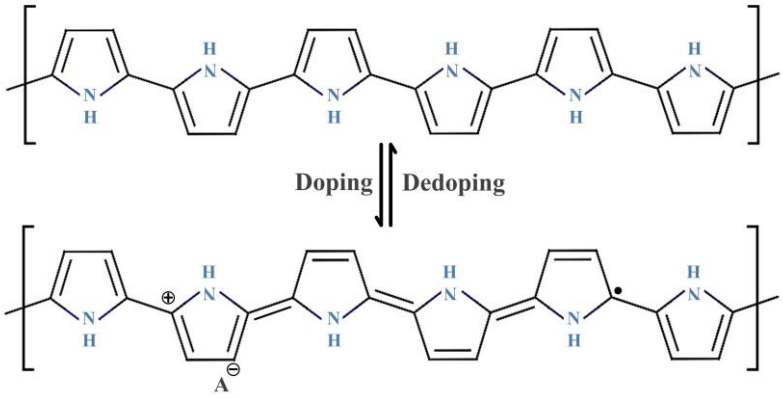

Scheme S1. The mechanism of doping/dedoping process of PPy.

For WO_3, the proton insertion/extraction reactions provide the capacitive performance. During the charging and discharging process, WO_3 converts into the electronically conductive tungsten bronze (H_xWO_3, $0<x<1$) reversibly as illustrated in Formula 1.

$$WO_3 + xH^+ + xe^- \leftrightarrow H_xWO_3 \qquad 1$$

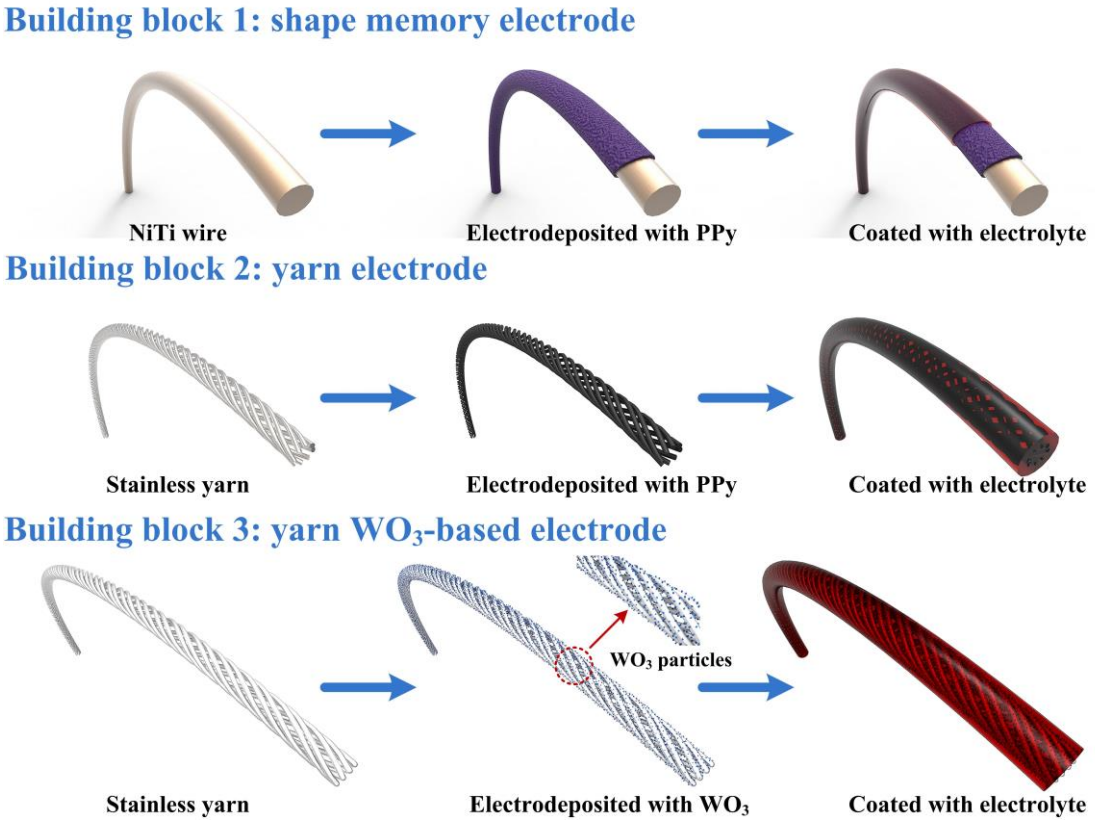

Fig. S1 Schematic demonstration of the fabrication of different building blocks.

Fig. S1 schematically demonstrates the fabrication of different build blocks. For building block 1, a NiTi wire, one kind of shape memory alloys, was used as the substrate. Owing to the outstanding electric conductivity, a layer of PPy as pseudocapacitive material was electrodeposited on the surface. After coating a certain thickness of solid electrolyte, a shape memory building block for C-SMSC was achieved. For building block 2, a conductive stainless yarn was used as the substrate. Then PPy was readily electrodeposited on its surface and follow by coating the electrolyte. Thus, a flexible yarn-based building block for C-SC yarn was obtained. For building block 3, the same conductive yarn was used as substrate and then electrodeposited with irregular WO_3 particles. A layer of solid electrolyte was subsequently coated on its surface. Thus, a WO_3-based building block for asymmetric C-SC was ready to use.

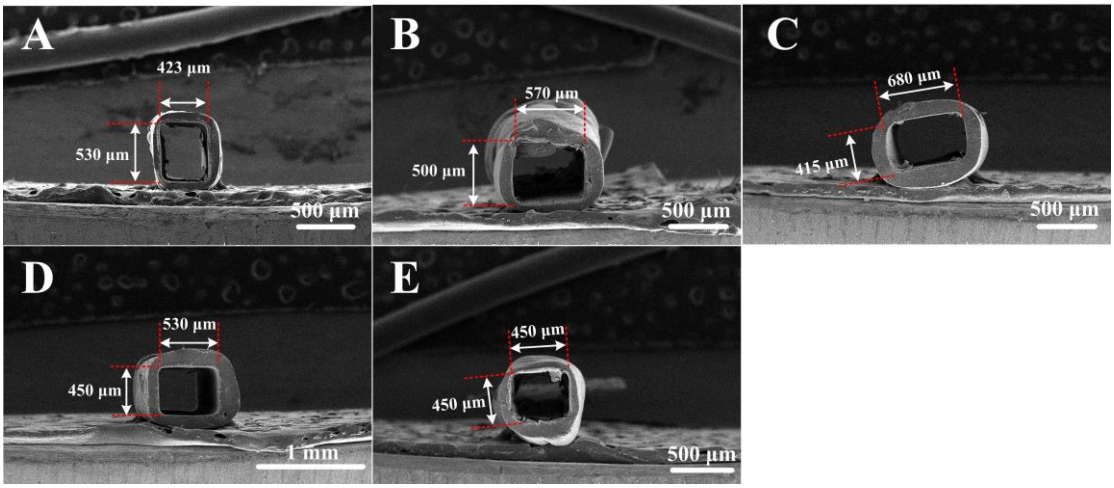

Fig. S2 Cross-section SEM images of PPy-based tubes with different shapes and sizes.

As shown in Fig. S2, rectangular and square PPy-based tubes with different sizes could be easily obtained by changing different molds/substrates, demonstrating the possibility of our reciprocal formwork construction technique in customized design.

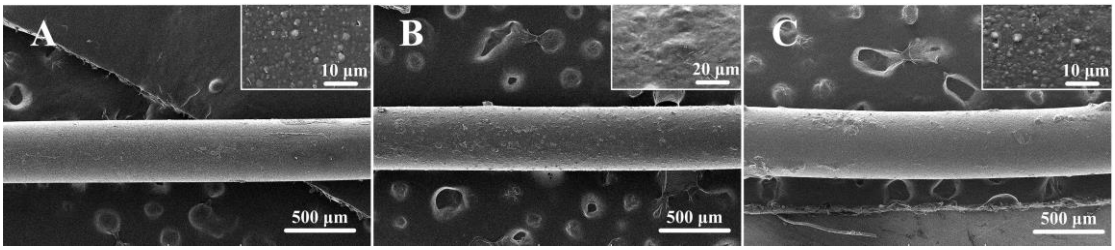

Fig. S3 SEM images of stainless wires after (A) PPy deposition, (B) Graphene paste coating, and (C) PPy deposition again. Insets are higher resolution images.

As shown in Fig. S3, after coating graphene paste, the rough surface of PPy-coated mold became smooth, whereas it became rough again after the second electrodeposition of PPy.

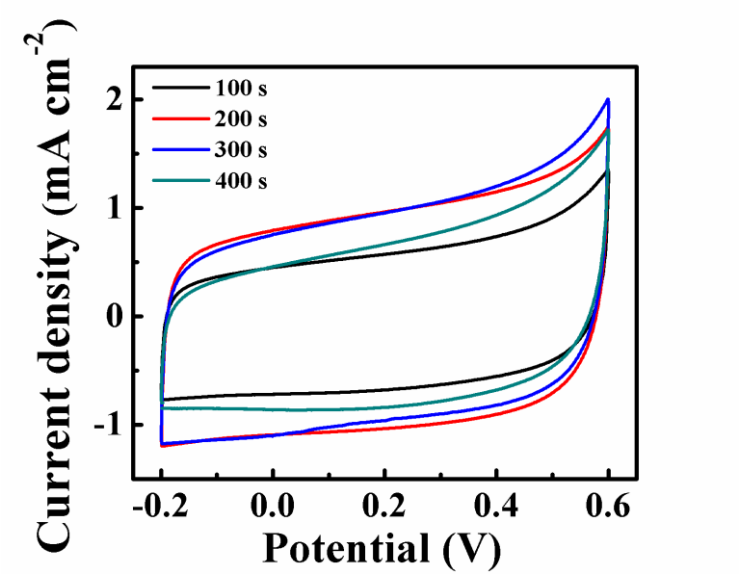

Fig. S4 CV curves of the molds/substrates with PPy electrodeposition duration from 100 to 400 s. The scan rate was 50 mV s^{-1}.

As shown in Fig. S4, when electrodeposition time was less than 300 seconds, the scan area increased as the duration increased. When the electrodepostion duration increased up to 400 seconds, the scan area of corresponding CV curve decreased obviously, indicating a reduced capacitance. So the total optimal deposition time for PPy was about 300 s. It is noted that in order to enhance the electrical conductivity and improve the cycling stability of PPy a graphene layer is introduced by a dip-coating method in the middle of electrodepostion process. For example, during 300 s electrodeposition, the process was stopped at 150 s and the mold was taken out and subsequently coated with the graphene paste. After drying, the electrodeposition was continued with the remaining 150 s.

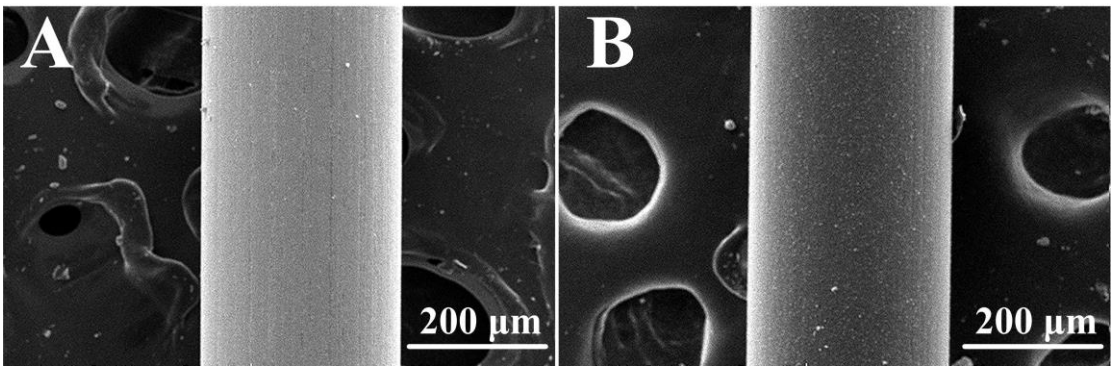

Figure S5. SEM images of the (A) Bare NiTi wire and (B) electrodeposited with PPy.

As shown in Fig. S5, the NiTi wire became rough after electrodepostion of PPy.

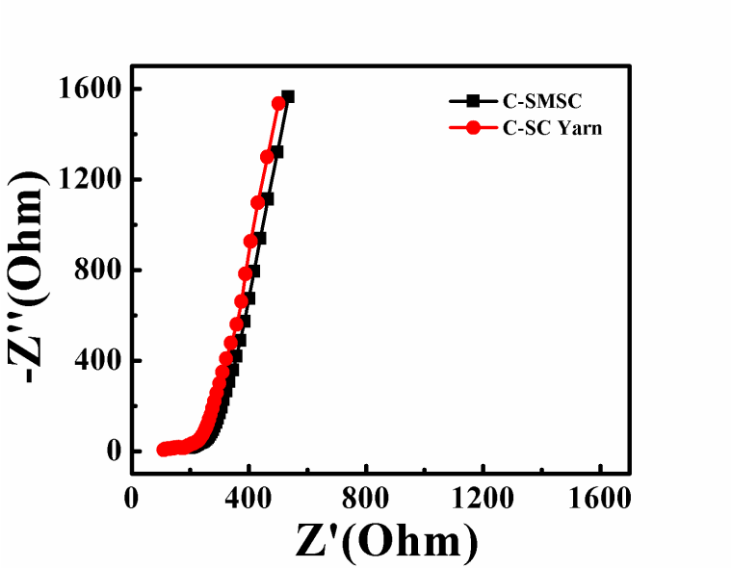

Fig. S6 Nyquist plots of the C-SMSC and C-SC yarn.

Fig. S6 showed the Nyquist plots of C-SMSC and C-SC yarn. The straight lines are nearly parallel to the imaginary axis, revealing ideal capacitive behavior of the devices. The system resistances (R_s) of C-SMSC and C-SC yarn are 124.1 Ω and 109.2 Ω, respectively; whereas the charge-transfer resistance (R_{ct}) are 72.6 Ω and 65.2 Ω, respectively.

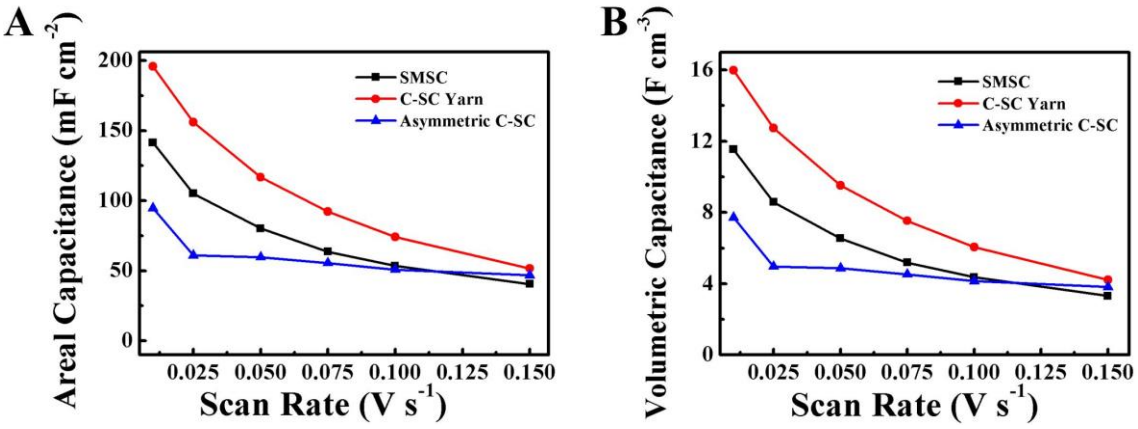

Fig. S7 (A) Areal capacitance and (B) volumetric capacitance *vs* scan rate of three prototypes.

Fig. S8 Calculation of the shape recovery ratio of C-SMSC.

Fig. S8 schematically demonstrates the calculation method of shape recovery ratio. A C-SMSC with a pre-designed linear shaped is firstly plastically deformed to an angle of θ_d (around 90^o), then it is heated up above the trigger temperature of shape memory effect (~35 ^{o}C), thus the deformed C-SMSC will restore to its original shape by recovering to an angle of θ_r. The configuration restoration capacity is evaluated by calculating the shape recovery ratio (R_r) according to the following equation: $R_r = \theta_r / \theta_d \times 100\%$.

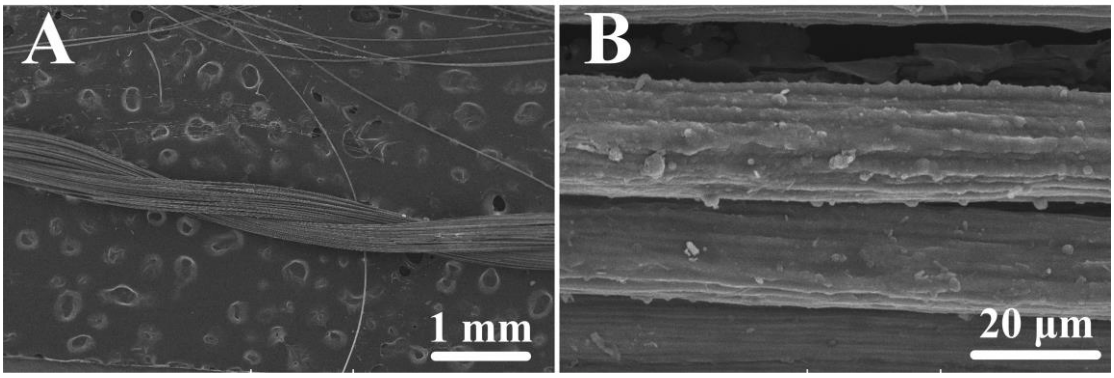

Fig. S9 SEM images of the (A) PPy electrodeposited yarn and (B) its higher resolution.

Fig. S9 showed the stainless yarn before and after electrodepostion of PPy. The smooth surface of yarn became rough after the deposition of PPy.

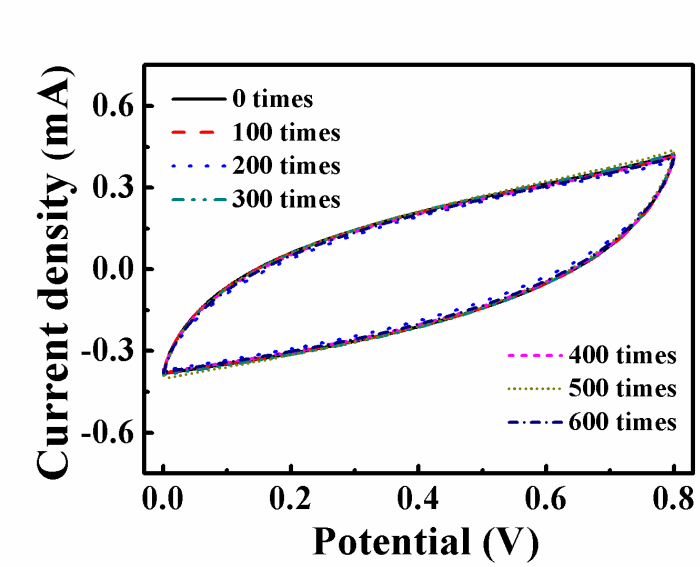

Fig. S10 CV curves of the C-SC yarn obtained at different bending cycles at a scan rate of 50 mV s^{-1}.

Fig. S10 showed the CV curves of C-SC yarn obtained at different bending cycles. No obvious deterioration of the CV curves could be observed. Even after up to 600 times bending, the CV curve still remained a symmetric quasi-rectangular shape.

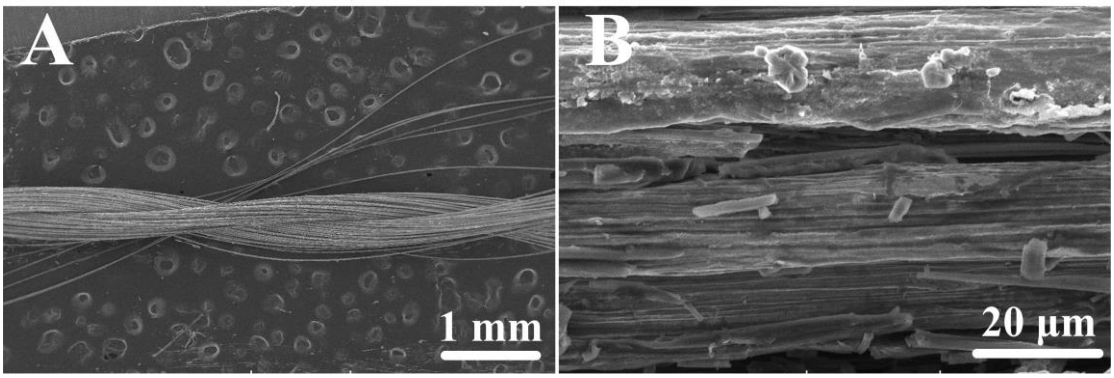

Fig. S11 SEM images of the (A) WO_3 electrodeposited yarn and (B) its higher resolution.

Fig. S11 showed the stainless yarn before and after electrodepostion of WO_3. After the deposition, irregular WO_3 particles were grown on tiny fibers of the yarn.

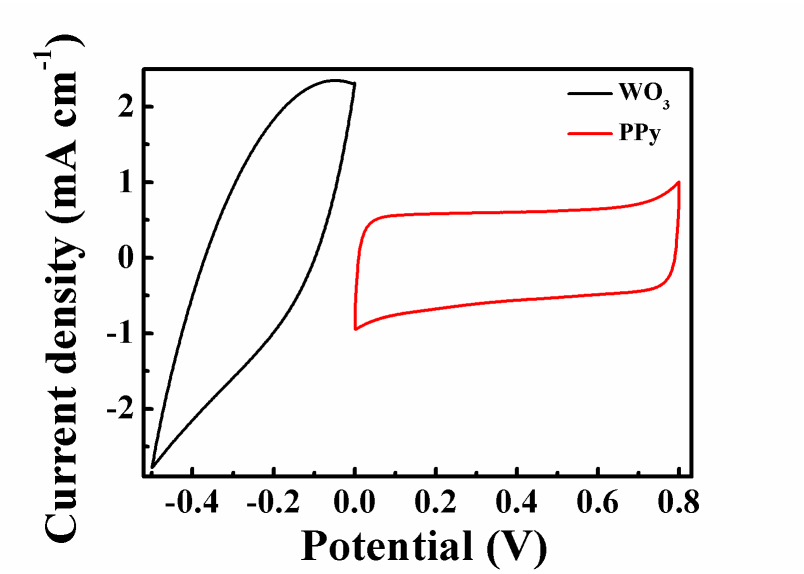

Fig. S12 CV curves of WO_3 electrodeposited yarn (negative electrode for asymmetric C-SC) and PPy electrodeposited stainless wire (positive electrode for asymmetric C-SC) in three-electrode system.

As shown in Fig. S12, the stable operating voltages for WO_3- and PPy-based electrodes are -0.5 to 0 V and 0 to 0.8 V, respectively. Thus, it is expected that the asymmetric C-SC could have a stable working voltage window of 1.3V. Besides, for assembling an asymmetric C-SC, the charge balance between negative and positive electrodes will follow the relationship $C_-V_- = C_+V_+$, where C_- and C_+ are the capacitances of the negative and positive electrodes, V_- and V_+ are the potential windows of the negative and positive electrodes. As discussed in the main text, our PPy-based tube was detached from the mold/substrate. Thus, the active material that contributed to capacitance should be the PPy layer adhered on solid electrolyte. So, we used a PPy-electrodeposited stainless wire (a nearly completed PPy-based formwork) to evaluate how much charges that could be stored in the positive electrodes, and thus as a reference for the assembling of asymmetric C-SC. According to Fig. S12, the length ratio of the electrodes was fixed to 0.957, in order to achieve a charge balance between WO_3-based building block and PPy-based tube.